J Neurophysiol 118: 634–646, 2017.
First published May 3, 2017; doi:10.1152/jn.00618.2016.

RESEARCH ARTICLE | *Sensory Processing*

Ube3a loss increases excitability and blunts orientation tuning in the visual cortex of Angelman syndrome model mice

Michael L. Wallace,[1] Geeske M. van Woerden,[5] Ype Elgersma,[5] Spencer L. Smith,[1,2,3,4] and Benjamin D. Philpot[1,2,3,4]

[1]*Curriculum in Neurobiology, University of North Carolina, Chapel Hill, North Carolina;* [2]*Department of Cell Biology and Physiology, University of North Carolina, Chapel Hill, North Carolina;* [3]*Neuroscience Center, University of North Carolina, Chapel Hill, North Carolina;* [4]*Carolina Institute for Developmental Disabilities, University of North Carolina, Chapel Hill, North Carolina; and* [5]*Department of Neuroscience, Erasmus MC University Medical Center, Rotterdam, The Netherlands*

Submitted 3 August 2016; accepted in final form 27 April 2017

Wallace ML, van Woerden GM, Elgersma Y, Smith SL, Philpot BD. *Ube3a* loss increases excitability and blunts orientation tuning in the visual cortex of Angelman syndrome model mice. *J Neurophysiol* 118: 634–646, 2017. First published May 3, 2017; doi:10.1152/jn.00618.2016.—Angelman syndrome (AS) is a neurodevelopmental disorder caused by loss of the maternally inherited allele of *UBE3A*. *Ube3a*$^{STOP/p+}$ mice recapitulate major features of AS in humans and allow conditional reinstatement of maternal *Ube3a* with the expression of Cre recombinase. We have recently shown that AS model mice exhibit reduced inhibitory drive onto layer (L)2/3 pyramidal neurons of visual cortex, which contributes to a synaptic excitatory/inhibitory imbalance. However, it remains unclear how this loss of inhibitory drive affects neural circuits in vivo. Here we examined visual cortical response properties in individual neurons to explore the consequences of *Ube3a* loss on intact cortical circuits and processing. Using in vivo patch-clamp electrophysiology, we measured the visually evoked responses to square-wave drifting gratings in L2/3 regular-spiking (RS) neurons in control mice, *Ube3a*-deficient mice, and mice in which *Ube3a* was conditionally reinstated in GABAergic neurons. We found that *Ube3a*-deficient mice exhibited enhanced pyramidal neuron excitability in vivo as well as weaker orientation tuning. These observations are the first to show alterations in cortical computation in an AS model, and they suggest a basis for cortical dysfunction in AS.

NEW & NOTEWORTHY Angelman syndrome (AS) is a severe neurodevelopmental disorder caused by the loss of the gene *UBE3A*. Using electrophysiological recording in vivo, we describe visual cortical dysfunctions in a mouse model of AS. Aberrant cellular properties in AS model mice could be improved by reinstating *Ube3a* in inhibitory neurons. These findings suggest that inhibitory neurons play a substantial role in the pathogenesis of AS.

Angelman syndrome; autism; *Ube3a*; visual cortex

ANGELMAN SYNDROME (AS) is a severe neurodevelopmental disorder characterized by cognitive disability, seizures, absence of speech, and high comorbidity with autism (Williams et al. 2006). The paternally inherited allele of *UBE3A* is epigenetically silenced in neurons. Therefore maternal deletions of the 15q11–q13 chromosomal regions or mutations specific to the *UBE3A* gene, which lies within that region, cause loss of neuronal UBE3A and result in AS (Kishino et al. 1997). A mouse model of AS, harboring a *Ube3a* null allele on the maternally inherited chromosome (*Ube3a*$^{m-/p+}$), recapitulates the major phenotypes seen in AS including ataxia, microcephaly, seizures, and cognitive disabilities (Jiang et al. 1998).

Layer (L)2/3 pyramidal neurons in visual cortex of *Ube3a*$^{m-/p+}$ mice have reduced inhibitory drive, which contributes to an excitatory/inhibitory imbalance (Wallace et al. 2012). Loss of inhibition is cell type specific, as pyramidal neurons, but not fast-spiking inhibitory interneurons, have reduced inhibitory inputs. Pyramidal neurons in *Ube3a*$^{m-/p+}$ mice also display increased intrinsic excitability, responding with more action potentials to a given depolarizing current injection (Wallace et al. 2012). Deficits in synaptic inhibition and cellular excitability may underlie cognitive disabilities in *Ube3a*$^{m-/p+}$ mice, given that balanced excitation and inhibition are crucial for many stages of sensory processing, circuit excitability, and neural computation (Isaacson and Scanziani 2011). Importantly, investigation of visual cortical plasticity in vivo has demonstrated that loss of *Ube3a* severely blunts ocular-dominance plasticity, a form of plasticity that is disrupted by changes in inhibition (Hensch et al. 1998; Sato and Stryker 2010; Yashiro et al. 2009). However, it remains unknown whether *Ube3a* loss disrupts cortical computations such as orientation tuning or intrinsic excitability in vivo.

An intensively studied computation performed by the visual cortex is orientation tuning, which is the preferential response of a neuron to bar-shaped visual stimuli presented at a particular angle (Hubel and Wiesel 1962). Orientation tuning largely emerges through specific circuitry in visual cortex (Hubel and Wiesel 1961; Lien and Scanziani 2013). Additionally, contrast sensitivity is a property of visual cortical neurons where responses increase nonlinearly with increasing luminance contrast (Albrecht and Hamilton 1982). Optogenetic modulation of local inhibitory neuron populations in cortex can alter orientation tuning and contrast sensitivity, indicating the importance of inhibitory drive to these visually evoked properties (Atallah

Address for reprint requests and other correspondence: B. D. Philpot, Univ. of North Carolina School of Medicine, 115 Mason Farm Rd., Chapel Hill, NC 27599-7545 (e-mail: bphilpot@med.unc.edu).

et al. 2012; Lee et al. 2012; Wilson et al. 2012). Therefore, we hypothesized that loss of inhibition in AS model mice may result in defective orientation tuning and contrast sensitivity.

Here we describe the effects of *Ube3a* loss on visually evoked responses, cellular excitability, and circuit excitability (UP/DOWN states), using in vivo whole cell recordings. We used a conditional *Ube3a* mouse line that restricts expression of *Ube3a* to cells expressing Cre, which mediates excision of a STOP cassette ($Ube3a^{STOP/p+}$). This line exhibits behavioral and synaptic phenotypes similar to the traditional $Ube3a^{m-/p+}$ mouse model of AS (Jiang et al. 1998; Judson et al. 2016; Silva-Santos et al. 2015). We found that *Ube3a* loss has no effect on the spontaneous activity of L2/3 regular-spiking (RS) neurons or on the local neural network as assayed by examination of UP/DOWN states. However, loss of *Ube3a* decreases the orientation tuning of L2/3 RS neurons without affecting contrast sensitivity. We show that reinstating *Ube3a* in GABAergic inhibitory neurons results in an intermediate effect on orientation tuning, suggesting a role for *Ube3a* in inhibitory interneurons and orientation tuning. Finally, increased excitability of RS neurons in $Ube3a^{STOP/p+}$ mice is rescued by reinstating *Ube3a* in GABAergic inhibitory neurons. Together these data identify a specific cortical processing deficit in an AS model.

MATERIALS AND METHODS

Animals

All studies were conducted with protocols approved by the University of North Carolina Animal Care and Use Committee. $Ube3a^{STOP}$ mice were on the 129Sv/Pas background and generated by the laboratory of Ype Elgersma (Silva-Santos et al. 2015). *Gad2-Cre* mice (Taniguchi et al. 2011) on the C57BL/6J background were obtained from the Jackson Laboratory (JAX no. 010802). All experiments were performed on mice obtained by crossing a female $Ube3a^{m+/STOP}$ mouse [which has normal expression of *Ube3a* in the brain (Silva-Santos et al. 2015)] with a male mouse heterozygous for *Gad2-Cre*. This cross produced four offspring genotypes: $Ube3a^{m+/p+} \pm$ *Gad2-Cre* mice (controls), $Ube3a^{STOP/p+}$ mice (AS model mice), and $Ube3a^{STOP/p+}$*::Gad2-Cre* mice (inhibitory neuron *Ube3a* reinstatement model). Experimental trios were littermates on a mixed 129Sv/Pas and C57BL/6J background, which had been backcrossed 2–6 generations onto C57BL/6J from the original 129Sv/Pas background. Mice of both sexes were used at postnatal day (P)70–110 at equivalent genotypic ratios and in strict compliance with animal protocols approved by the Institutional Animal Care and Use Committee of the University of North Carolina at Chapel Hill.

In Vivo Whole Cell Physiology

Mice were anesthetized with 5 mg/kg chlorprothixene followed by 0.9–1.2 g/kg urethane injected intraperitoneally (ip). Secretions were reduced by administration of atropine (0.3 mg/kg ip). Mice were stereotaxically secured after reaching a surgical plane of anesthesia (~30 min), and then a uniform layer of water-based ophthalmic ointment was applied to the cornea to prevent drying. A homeothermic blanket (FHC, Bowdoinham, ME) maintained the animal's body temperature within a physiological range (37 ± 0.5°C). Incised tissue was locally anesthetized with bupivacaine (0.25% wt/vol), and a ~1.5-mm^2 craniotomy was performed over primary visual cortex (2.5 mm lateral to midline, 0.5 mm anterior to lambda). A durotomy was then made (~0.2 mm^2) and covered with artificial cerebrospinal fluid (in mM: 124 NaCl, 3 KCl, 1.25 NaH_2PO_4, 26 $NaHCO_3$, 1 $MgCl_2$, 2 $CaCl_2$ and 20 glucose bubbled with 95% O_2-5% CO_2 before application) to prevent drying.

Whole cell recordings were made with the blind-patch method as described previously (Margrie et al. 2002). Patch pipettes were pulled from thick-walled borosilicate glass (P2000; Sutter Instruments, Novato, CA). Open tip resistances were between 5 and 8 MΩ when pipettes were filled with the internal solution containing (in mM) 135 K-gluconate, 6 KCl, 10 HEPES, 0.1 EGTA, 4 Mg-ATP, 3 Na-GTP, 8 Na-phosphocreatine, and 0.05% neurobiotin, with pH adjusted to 7.25 with 1 M KOH and osmolarity adjusted to ~295 mosM by addition of sucrose. The micromanipulator (Luigs and Neumann, Germany) was arranged for electrodes to penetrate the brain perpendicular to the cortical surface, and depth measurements were made from the pial surface to the recorded cell. All of the neurons included for analysis were between 100 and 400 μm from the pial surface. Current-clamp recordings were performed with a Multiclamp 700A amplifier (Molecular Devices), and data were acquired at 20 kHz and Bessel filtered at 10 kHz. Series resistance was 39 ± 1.3 (n = 42), 39 ± 1.4 (n = 32), and 32 ± 1.6 (n = 30) MΩ for recordings in control, $Ube3a^{STOP/p+}$, and $Ube3a^{STOP/p+}$*:: Gad2-Cre* mice, respectively. Data were discarded if the series resistance changed >30% during the course of the recording. Resting membrane potential was assessed immediately after break-in, and membrane resistance was measured as the steady-state membrane potential in response to a 50-pA hyperpolarizing current step during a DOWN state. After break-in, we waited several minutes to allow for synaptic activity (and UP/DOWN states) to return from excess extracellular potassium before we conducted intrinsic excitability experiments (Fig. 1). Reported voltages were not corrected for junction potential. All analyses were performed in Clampfit 10.2 or with custom routines written in MATLAB (MathWorks).

Visual Stimulation

Visual stimulus presentation was controlled by routines written in MATLAB (MathWorks) with the Psychophysics Toolbox extensions (Brainard 1997). Square-wave gratings (0.04 cycles/° at 2 Hz) were displayed on an LCD screen (Dell; 33 × 27 cm, 75 Hz refresh rate, mean luminance ~46 cd/m^2) centered 20 cm from the animal's eyes. The screen was angled to stimulate the contralateral (left) eye for the experiments, but the ipsilateral eye was not covered. Visual stimuli were presented in a shuffled order. To acquire orientation tuning curves, each of eight different orientations was presented at least six times. The contrast-response curves were obtained by showing the preferred orientation at eight contrast levels logarithmically spanning the range from 1% to 100% contrast.

Data Analysis

Spontaneous activity. Spontaneous spiking rates and UP/DOWN states were analyzed during presentation of a gray screen and calculated over a period of ~5 min. Only cells that had a clear bimodal distribution of V_m were used for analysis (68 of 102 cells passed this criterion). For UP vs DOWN state detection, traces were low-pass filtered at 3 Hz and the mean and standard deviation of the voltage were calculated. UP state threshold was defined as the mean voltage plus half the standard deviation of the voltage. UP states were detected whenever the membrane potential crossed this defined threshold and remained above the threshold for at least 150 ms (Beltramo et al. 2013; Gonçalves et al. 2013). Periods not detected as UP states were considered DOWN states. These parameters were empirically found to detect UP and DOWN states accurately.

Spectral analysis. Recorded voltage signals were processed off-line with custom-written scripts in MATLAB (MathWorks) (Sellers et al. 2013). Figures represent the average (± SE) of the median power for each frequency for an entire recording session from a single neuron. Time-dependent frequency content was determined by convolution of voltage signals with a family of Morlet wavelets (0.5–100 Hz, step

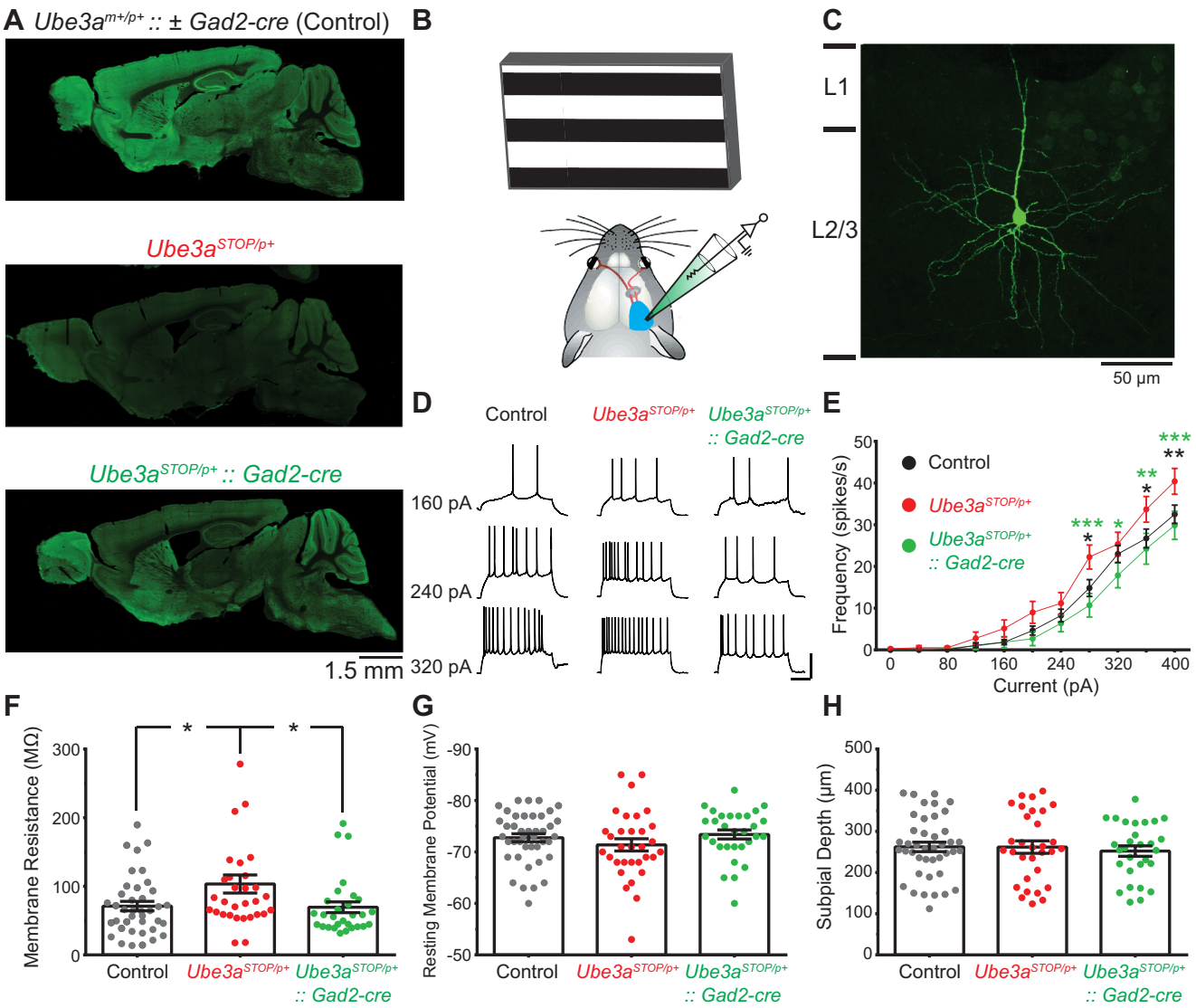

Fig. 1. Reinstatement of *Ube3a* in *Gad2-Cre+* inhibitory neurons normalizes intrinsic excitability and membrane resistance in L2/3 RS neurons of $Ube3a^{STOP/p+}$ mice. *A*: sagittal brain sections from control, $Ube3a^{STOP/p+}$, and $Ube3a^{STOP/p+}$*::Gad2-Cre* mice immunostained for UBE3A. *B*: schematic of in vivo whole cell recording configuration. *C*: sample image of a L2/3 pyramidal neuron that was recorded, filled with neurobiocytin, and stained post hoc. *D*: sample recordings from L2/3 regular-spiking (RS) pyramidal neuron in response to increasing current injections (scale bar 40 mV, 100 ms). *E*: average frequency vs. current curves from whole cell recordings in control ($n = 42$ cells), $Ube3a^{STOP/p+}$ ($n = 34$), and $Ube3a^{STOP/p+}$*:: Gad2-Cre* ($n = 31$) mice. Note that all significance values are post hoc comparisons between $Ube3a^{STOP/p+}$ group and either control (black asterisk) or $Ube3a^{STOP/p+}$*::Gad2-Cre* (green asterisk) groups. *F*: membrane resistance measured during a DOWN state in RS neurons from control ($n = 39$), $Ube3a^{STOP/p+}$ ($n = 31$), and $Ube3a^{STOP/p+}$*:: Gad2-Cre* ($n = 29$) mice. *G*: membrane potential during a DOWN state in L2/3 RS neurons from control ($n = 42$), $Ube3a^{STOP/p+}$ ($n = 32$), and $Ube3a^{STOP/p+}$*:: Gad2-Cre* ($n = 30$) mice. *H*: depth from the pial surface of all RS cells recorded in L2/3 from control ($n = 42$), $Ube3a^{STOP/p+}$ ($n = 31$), and $Ube3a^{STOP/p+}$*:: Gad2-Cre* ($n = 29$) mice. $^*P < 0.05$, $^{**}P < 0.01$, $^{***}P < 0.001$ with post hoc test for significance.

width 0.5 Hz) with normalized amplitude, providing an optimal trade-off between time and frequency uncertainty (Goupillaud et al. 1984; Sohal et al. 2009). Total power for each frequency band was calculated by taking the median value across an epoch (i.e., UP state or DOWN state) for the included frequencies (delta 0.5–4 Hz, theta 4.5–8 Hz, alpha 8.5–12 Hz, beta 12.5–29.5 Hz, gamma 30–80 Hz) (Sellers et al. 2013). In Fig. 4, analysis of the delta frequency band was limited to 2–4 Hz to avoid including edge artifacts from the visual stimulation occurring for 1 s.

Visually evoked responses. The spiking visual response to a given stimulus was the average rate over the stimulus duration (1 s). The subthreshold (membrane potential) visual response to a given stimulus was measured as the "Area" ($V \times s$) during the stimulus duration. For analysis of subthreshold responses, the "baseline" was calculated for each neuron as the average membrane potential during a DOWN state, and recordings were filtered at 100 Hz to remove spikes. The *F1* (modulated) and *F0* (mean) components of the subthreshold response were calculated as shown in Fig. 7*A*. Orientation selectivity index (OSI) was calculated as (1 − the circular variance) (Ringach et al. 1997). Orientation selectivity was also examined with peak-to-orthogonal ratios (Fig. 6*H*) $(R_{pref} - R_{ortho})/(R_{pref} + R_{ortho})$, where R_{pref} is the response to the preferred direction and R_{ortho} is the response 90° away from the preferred direction. Direction selectivity index (DSI) was calculated as $(R_{pref} - R_{null})/(R_{pref} + R_{null})$, where R_{null} is the response 180° away from the preferred direction (Niell and Stryker 2008). The responses to the eight grating directions were fit with a sum of two Gaussians (Fig. 6). The Gaussians were centered 180° apart and had the same tuning sharpness (σ), but amplitudes for each of the two Gaussians were varied to fit the data. The fitting routine used a least-squares method to minimize the Cartesian distance

between the model and the data (Carandini and Ferster 2000). To examine only robustly tuned neurons, we calculated the normalized (to the mean firing rate of the preferred direction) residuals of the fit. We then applied a criterion of <0.125 normalized residual to all the cells and reanalyzed the data (Fig. 6*G*) (Cottam et al. 2013). The tuning sharpness, or half-width at half height (HWHH), was measured as $\sigma \times [2 \ln(2)]^{1/2}$. Contrast-response curves were fit with a hyperbolic ratio equation (Albrecht and Hamilton 1982): $R(C) = R_{max}c^n/C_{50}^n + c^n) + R_{offset}$ where c is contrast, C_{50} is the semisaturation contrast, n is the fitting exponent that describes the shape of the curve, R_{max} determines the gain, and R_{offset} is the baseline response.

Immunohistochemistry

For a subset of recordings where the recorded neuron was reconstructed, mice were killed by administration of pentobarbital (40 mg/kg) and subsequently intracardially perfused with ~80 ml of 4% paraformaldehyde (0.1 M, pH 6.8). Brains were then postfixed for 24 h and sliced coronally at 100 μm. The slices were then permeabilized in 1% Triton X for 12 h and incubated at 4°C for 12 h in Alexa 488-conjugated streptavidin (1:1,000), 5% normal goat serum, and 0.1% Triton X. For Fig. 1, sagittal sections were cut at 40–60 μm and then washed in 0.1 M PBS, permeabilized in 0.2% Triton X, and blocked in 5% normal goat serum. Primary antibody (mouse anti-Ube3a, 1:750; Sigma) was incubated for 48 h at 4°C, and secondary antibody (goat anti-mouse Alexa 488; A21131) was incubated at 1:500 for 1 h at room temperature. Sections were imaged on a Zeiss LSM 710 confocal microscope.

Statistics

The D'Agostino and Pearson omnibus normality test was used to assess normality of data sets. If data were normally distributed, we used a one- or two-way analysis of variance (ANOVA) with a Tukey's post hoc test to test for significance if an overall significant effect was found. If data were not normally distributed, we used the Kruskal-Wallis test with Dunn's post hoc test to test for significance. The statistical measure and *P* value for each comparison are stated in each figure legend. For sample sizes reported in figures, *n* represents number of neurons recorded. One to four neurons were recorded per animal. Graphs represent the mean, and error bars represent the SE. For all figures significance values are post hoc comparisons. All statistics were performed in GraphPad Prism 6.

RESULTS

Intrinsic Excitability of L2/3 Regular-Spiking Neurons in Vivo

To examine the role of UBE3A in cortical neurons in vivo we took advantage of *Ube3a*$^{STOP/p+}$ mice modeling AS. In these mice, *Ube3a* can be conditionally reinstated by Cre-mediated removal of a STOP cassette inserted between exons 3 and 4 of *Ube3a* (Silva-Santos et al. 2015). We used immunocytochemistry to verify that UBE3A levels were high in control mice with intact *Ube3a* (*Ube3a*$^{m+/p+}$ ± *Gad2-Cre*) but was absent in neurons of *Ube3a*$^{STOP/p+}$ mice (Fig. 1*A*). *Ube3a* expression was effectively reinstated in forebrain inhibitory interneurons, but not pyramidal neurons, in *Ube3a*$^{STOP/p+}$*:: Gad2-Cre* mice. This is consistent with previous observations that the *Gad2-Cre* line expresses Cre in almost all GABAergic neurons from mid- to late embryonic development (Taniguchi et al. 2011) and is also consistent with our previous studies in this mouse line (Judson et al. 2016).

We performed in vivo whole cell recordings from anesthetized mice to examine the contributions of UBE3A to intrinsic excitability and visually evoked responses of L2/3 cortical neurons in an intact cortical circuit (Fig. 1*B*). We chose to record from L2/3 neurons in the visual cortex as their responses to visual stimulation are well characterized (Niell and Stryker 2008). Moreover, visual cortical deficits in synaptic function, anatomy, and critical period plasticity have been identified in AS model mice (Wallace et al. 2012; Yashiro et al. 2009).

L2/3 pyramidal neurons were identified by cortical depth and by their regular spiking characterized by an adapting firing pattern to depolarizing current injections (Fig. 1*D*). A subset ($n = 6$ cells) of these neurons were filled with neurobiocytin, stained post hoc, and found to exhibit pyramidal morphology and spinous dendrites (Fig. 1*C*). All of the neurons included for analysis were between 100 and 400 μm from the pial surface (Fig. 1*H*). Given these parameters, it is likely that the vast majority, if not all, of the neurons included in this study are L2/3 pyramidal neurons, which are referred to here as regular-spiking (RS) neurons.

Similar to in vitro results from *Ube3a*$^{m-/p+}$ mice (Wallace et al. 2012), we found that in vivo L2/3 RS neurons of *Ube3a*$^{STOP/p+}$ mice had increased spiking activity following current injection compared with control mice (Fig. 1, *D* and *E*). Reinstatement of *Ube3a* in Gad2-Cre-positive (GABAergic) neurons in *Ube3a*$^{STOP/p+}$*:: Gad2-Cre* mice normalized intrinsic excitability to control levels (Fig. 1*E*), indicating that this effect was non-cell-autonomous. *Ube3a*$^{STOP/p+}$ mice also showed increased membrane resistance compared with control mice, which was also normalized in *Ube3a*$^{STOP/p+}$*:: Gad2-Cre* mice (Fig. 1*F*). There were no apparent differences between groups in resting membrane potential (Fig. 1*G*). Thus, the increase in intrinsic excitability observed in *Ube3a*$^{STOP/p+}$ mice is likely due to increased membrane resistance.

Spontaneous Cortical Network Activity and Spiking Activity in Ube3a$^{STOP/p+}$ *Mice*

The cortex of anesthetized mice commonly exhibits a slow (<1 Hz) network oscillation (Steriade et al. 1993), which consists of rhythmic cycles of synaptically mediated depolarizations and spiking activity (UP states) followed by reduced synaptic input and termination of spiking activity (DOWN states) (Haider and McCormick 2009). The slow oscillation requires balanced fluctuations of excitation and inhibition; thus altered UP and DOWN states can indicate changes in excitability of the local network (Sanchez-Vives and McCormick 2000; Shu et al. 2003). We hypothesized that UP and DOWN states may be altered given the excitatory/inhibitory imbalance we previously observed in vitro in AS model mice and that such deficits have been observed in other models of neurodevelopmental disorders (Gibson et al. 2008; Hays et al. 2011; Paluszkiewicz et al. 2011).

We measured network oscillations and spiking activity in L2/3 RS neurons during presentation of a gray screen as a metric of spontaneous local network activity (Fig. 2, *A* and *B*). Spiking activity was very low in L2/3 RS neurons (Fig. 2*C*), consistent with previous reports (de Kock et al. 2007; Wolfe et al. 2010). Average spontaneous firing rates did not differ between experimental groups, and many (~50%) neurons did not have appreciable spontaneous spiking events (Fig. 2*C*). We

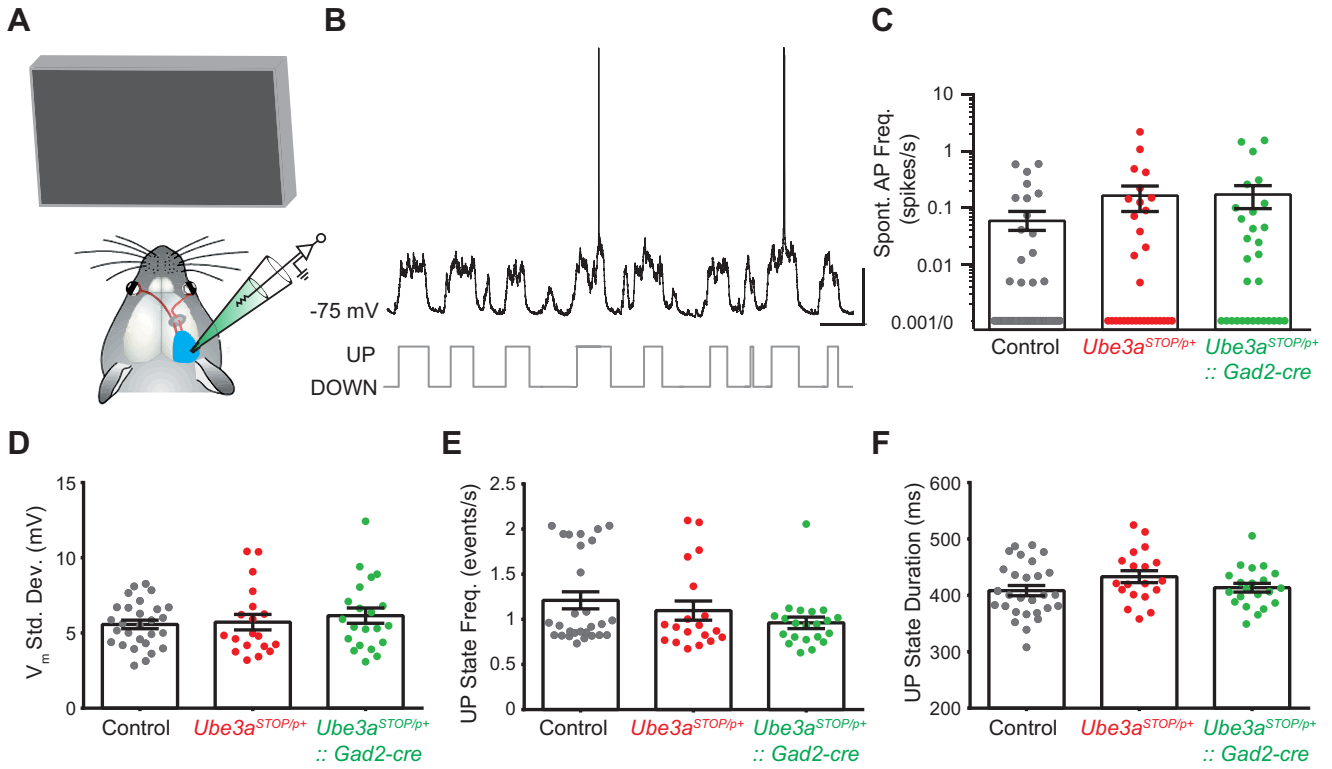

Fig. 2. Global *Ube3a* deletion does not affect spontaneous spiking rates and oscillatory activity in L2/3 RS neurons. *A*: schematic of recording configuration during spontaneous activity (note that animal is presented with a gray screen stimulus). *B*: sample recording of a spontaneously active L2/3 RS neuron (*top*) and an example of automated detection of UP/DOWN states (*bottom*) (scale bars = 1 s, 25 mV). *C*: spontaneous spiking activity rates for all RS neurons recorded in L2/3 of control ($n = 41$), *Ube3a*$^{STOP/p+}$ ($n = 31$), and *Ube3a*$^{STOP/p+}$*::Gad2-Cre* ($n = 30$) mice (note that points at "0.001/0" represent neurons that did not exhibit spontaneous spiking activity during the recording session) (Kruskal-Wallis test, $P = 0.315$). *D*: standard deviation of the membrane voltage for all RS neurons recorded in L2/3 for control ($n = 28$), *Ube3a*$^{STOP/p+}$ ($n = 19$), and *Ube3a*$^{STOP/p+}$*::Gad2-Cre* ($n = 21$) mice (ANOVA, $P = 0.59$). *E*: UP state frequency for control ($n = 28$), *Ube3a*$^{STOP/p+}$ ($n = 19$), and *Ube3a*$^{STOP/p+}$*::Gad2-Cre* ($n = 21$) mice (Kruskal-Wallis test, $P = 0.446$). *F*: UP state duration for control ($n = 28$), *Ube3a*$^{STOP/p+}$ ($n = 19$), and *Ube3a*$^{STOP/p+}$*::Gad2-Cre* ($n = 21$) mice (ANOVA, $P = 0.161$).

measured UP state frequency and duration, and they were not different between groups (Fig. 2, *E* and *F*). The standard deviation of the membrane voltage was also similar, indicating that the voltage difference between UP and DOWN states was similar between groups (Fig. 2*D*). These data suggest that, despite an apparent excitatory/inhibitory imbalance in AS model mice, spontaneous network activity and baseline firing rates are not altered by the loss of *Ube3a* expression.

Spectral Analysis of Membrane Voltage During Spontaneous Activity in Ube3a$^{STOP/p+}$ *Mice*

EEG/ECoG recordings of cortical network oscillations are disrupted in AS individuals and model mice (Colas et al. 2005; Jiang et al. 1998; Thibert et al. 2013). As membrane potential fluctuations in single neurons reflect local network synchrony and oscillations (Poulet and Petersen 2008), we performed a spectral analysis of the membrane potential of L2/3 RS neurons during presentation of a gray screen to determine whether we could detect altered cortical oscillations in *Ube3a*$^{STOP/p+}$ mice (Fig. 3*B*). We observed no significant changes in delta (0.5–4 Hz), theta (4.5–8 Hz), alpha (8.5–12 Hz), beta (12.5–29.5 Hz), or gamma (30–80 Hz) frequency bands in *Ube3a*$^{STOP/p+}$ mice compared with control mice or *Ube3a*$^{STOP/p+}$*:: Gad2-Cre* mice (Fig. 3*C*). As UP and DOWN states have different biases for high- and low-frequency bands (Beltramo et al. 2013), we performed a spectral analysis on the UP and DOWN states separately in addition to the overall spectral analysis of membrane potential (Fig. 3, *D* and *E*). Consistent with previous reports, UP states carried more power in the gamma bands than DOWN states; however, we did not find any changes in spectral power between the experimental groups for either UP states or DOWN states. Our data suggest that, at least in anesthetized mice, cortical oscillations are normal in *Ube3a*$^{STOP/p+}$ mice.

Spectral Analysis of V_m During Visual Stimulation

The presentation of visual stimuli increases gamma (30–80 Hz) synchrony in visual cortex (Eckhorn et al. 1988). Additionally, activating cortical parvalbumin-positive GABAergic neurons increases gamma band activity and improves behavioral performance (Cardin et al. 2009). Disruptions in gamma synchrony have been observed in many psychiatric disorders, including autism (Orekhova et al. 2007). Therefore, we tested whether increased gamma power induced by visual stimulation was affected by loss of *Ube3a* (Fig. 4*A*). We measured the spectral power preceding and during 1 s of visual stimulation with drifting gratings and calculated the percent change in power with visual stimulation at each frequency. Consistent with previous reports (Eckhorn et al. 1988; Sellers et al. 2013), we observed an increase in power in the gamma band with visual stimulation; however, we observed no differences between experimental groups (Fig. 4, *B* and *C*). Therefore, gamma oscillations induced by visual stimulation in anesthetized mice are unaffected by *Ube3a* loss.

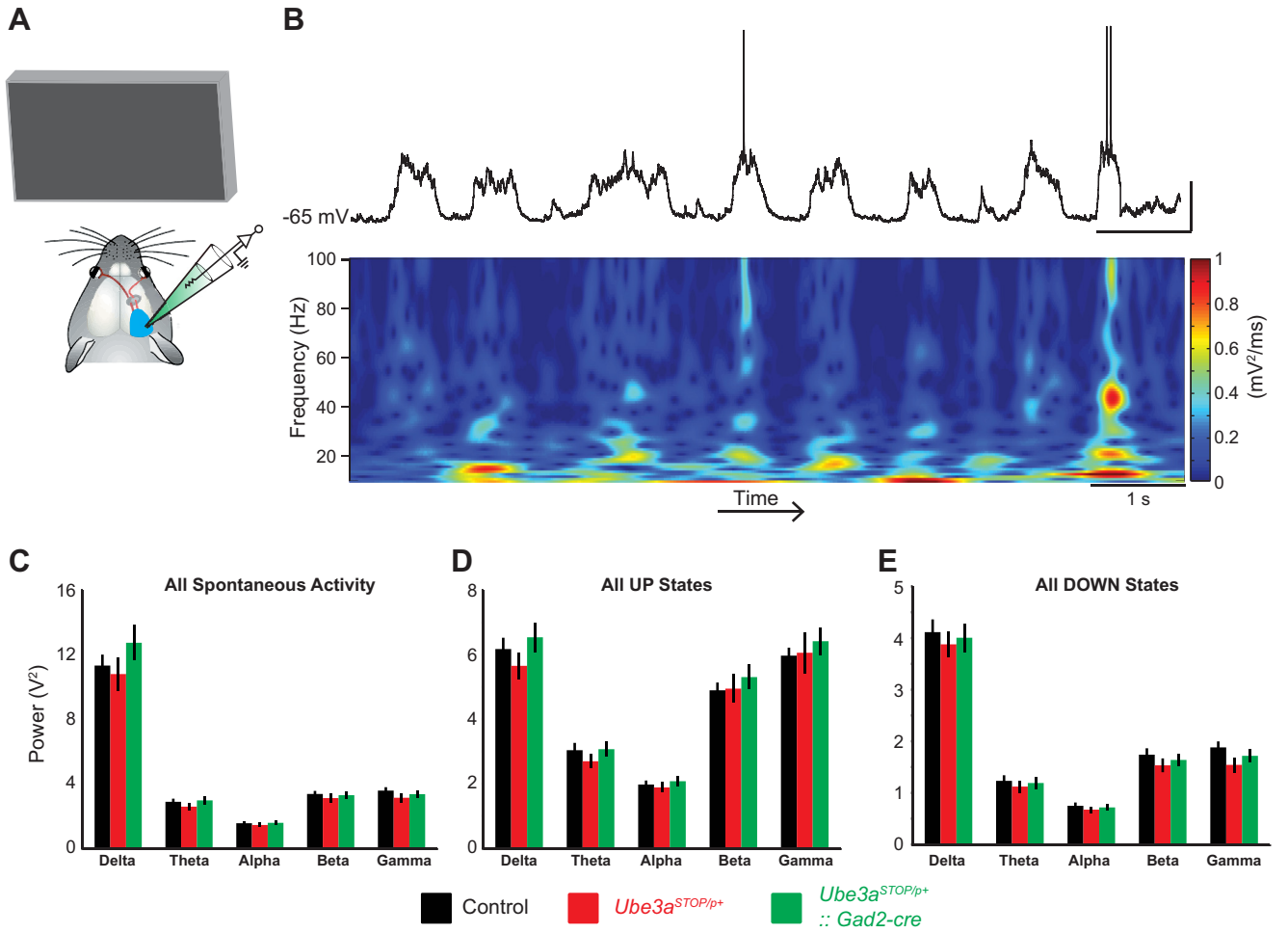

Fig. 3. Spectral analysis of spontaneous UP/DOWN states in L2/3 RS neurons. *A*: schematic of recording configuration during spontaneous activity (note that animal is presented with a gray screen stimulus). *B*: sample recording of a spontaneously active L2/3 RS neuron (*top*) and corresponding spectrogram (*bottom*) (scale bar = 1 s, 20 mV). *C*: average power spectrum of spontaneous activity of individual L2/3 RS neurons for control ($n = 24$), *Ube3a*$^{STOP/p+}$ ($n = 19$), and *Ube3a*$^{STOP/p+}$*::Gad2-Cre* ($n = 18$) mice. Frequency ranges are defined as delta (0.5–4 Hz), theta (4.5–8 Hz), alpha (8.5–12 Hz), beta (12.5–29.5 Hz), and gamma (30–80 Hz) (2-way ANOVA, $P = 0.462$). *D*: average power spectrum of UP states of individual L2/3 RS neurons for control ($n = 24$), *Ube3a*$^{STOP/p+}$ ($n = 19$), and *Ube3a*$^{STOP/p+}$*::Gad2-Cre* ($n = 18$) mice (2-way ANOVA, $P = 0.58$). *E*: average power spectrum of DOWN states of individual L2/3 RS neurons for control ($n = 24$), *Ube3a*$^{STOP/p+}$ ($n = 19$), and *Ube3a*$^{STOP/p+}$*::Gad2-Cre* ($n = 18$) mice (2-way ANOVA, $P = 0.53$).

Effects of Ube3a Loss on Contrast Sensitivity in L2/3 Regular-Spiking Neurons

Contrast sensitivity is a property of L2/3 RS neurons where responses increase nonlinearly with increasing luminance contrast (Albrecht and Hamilton 1982). To examine whether the loss of *Ube3a* altered contrast sensitivity, we performed whole cell recordings while presenting mice with drifting gratings of differing contrast shown at the neuron's predetermined preferred orientation (Fig. 5*A*). Spiking contrast responses did not differ between groups (Fig. 5, *B–D*). The same was true for subthreshold contrast response (Fig. 5, *E–G*). In conclusion, *Ube3a* loss does not affect the contrast response of L2/3 RS neurons. This result confirms grossly normal function of visual circuitry in *Ube3a* mice.

Effects of Ube3a Loss on Orientation Tuning in L2/3 Regular-Spiking Neurons

L2/3 RS neurons were recorded while drifting gratings were presented in the visual field of the animal. There was no difference in the average subthreshold response amplitude (control, 28.9 ± 1.6 mV; *Ube3a*$^{STOP/p+}$ 28.1 ± 2.4 mV; *Ube3a*$^{STOP/p+}$*::Gad2*-Cre 31.2 ± 2.2 mV) or frequency of spiking (Fig. 6*C*) of L2/3 neurons to the visual stimulus. First, we compared tuning sharpness of spiking tuning curves (Fig. 6*D*). Neurons in *Ube3a*$^{STOP/p+}$ mice had significantly broader tuning than in *Ube3a*$^{STOP/p+}$*::Gad2*-Cre mice ($P < 0.05$) and showed a trend for broader tuning compared with control mice ($P = 0.16$) (Fig. 6*D*). The OSI of spiking tuning curves was significantly decreased in the *Ube3a*$^{STOP/p+}$ mice compared with control mice ($P < 0.05$) (Fig. 6*E*). *Ube3a*$^{STOP/p+}$*::Gad2-Cre* mice showed an intermediate effect in OSI that was not statistically different from control mice or *Ube3a*$^{STOP/p+}$ mice ($P = 0.48$ and 0.29, respectively) (Fig. 6*E*). To investigate the OSI and tuning sharpness of robustly tuned neurons, we examined robustness of the curve fit (sum of two Gaussians, see MATERIALS AND METHODS) by calculating the normalized (to the mean firing rate of the preferred direction) residuals of the fit. We applied a criterion of <0.125 normalized residual to all cells and analyzed neurons that passed this criterion (Fig. 6*G*) (Cottam et al. 2013). Robustly tuned *Ube3a*$^{STOP/p+}$ neurons

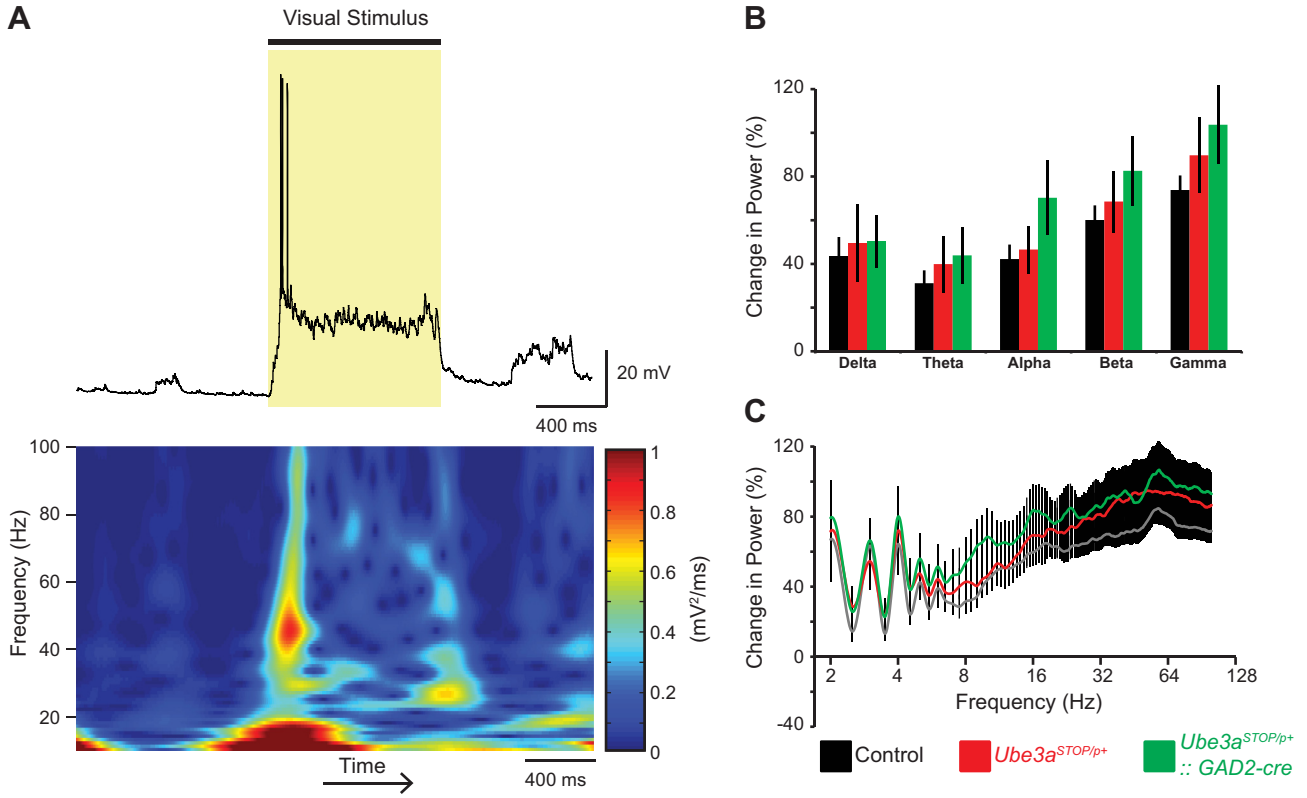

Fig. 4. Spectral power changes induced with visual stimulation. *A*: sample recording of a L2/3 RS neuron during 1 s of visual stimulation (shaded region, *top*) and corresponding spectrogram of recording (*bottom*). *B*: average change in power with visual stimulation at different frequency bands for control ($n = 31$), *Ube3a*$^{STOP/p+}$ ($n = 26$), and *Ube3a*$^{STOP/p+}$*::Gad2-Cre* ($n = 23$) mice (2-way ANOVA, $P = 0.542$). Frequency ranges are defined as delta (2–4 Hz), theta (4.5–8 Hz), alpha (8.5–12 Hz), beta (12.5–29.5 Hz), and gamma (30–80 Hz). *C*: average change in power with visual stimulation for all frequencies for control ($n = 31$), *Ube3a*$^{STOP/p+}$ ($n = 26$), and *Ube3a*$^{STOP/p+}$*:: Gad2-Cre* ($n = 23$) mice.

showed decreased OSI and increased tuning width compared with control mice ($P < 0.05$) (Fig. 6, *F* and *G*). To examine robustly responsive neurons more closely, we performed ANOVA on the spiking responses to visual stimulation. Neurons that did not show statistically distinguishable responsiveness to any particular orientation were excluded from subsequent analysis (Fig. 6*H*). Similarly to all neurons grouped together, robustly responsive *Ube3a*$^{STOP/p+}$ neurons also showed decreased OSI compared with control mice ($P < 0.05$)(Fig. 6*H*). As a final measure of orientation tuning we calculated the preferred-to-orthogonal ratios for all cells and compared the groups using this metric. Surprisingly, there were no statistically significant differences between groups for this measure of orientation tuning (Fig. 6*I*). However, trends reflected what we have observed with OSI ($P = 0.15$). Finally, we calculated the DSI for the spiking responses, and this metric was not measurably different between groups (Fig. 6*J*). Together these data strongly suggest that *Ube3a* loss results in weaker orientation tuning in L2/3 RS neurons that are robustly responsive and tuned to orientation.

Subthreshold (i.e., membrane potential) responses recorded in L2/3 RS neurons also showed orientation tuning, albeit less sharply tuned than spiking responses (Fig. 7, *D* and *E*) (Smith et al. 2013). In response to drifting gratings the membrane potential will fluctuate in amplitude at the same temporal frequency (2 Hz) of the stimulus (Fig. 7, *A* and *B*). The difference between the peak and trough is the *F1* (or frequency modulated) component, whereas the mean membrane potential during the stimulus is the *F0* component. The *F1* component has been shown to be more highly tuned for orientation than the "Area" or the *F0* measurement (Carandini and Ferster 2000; Lien and Scanziani 2013; Niell and Stryker 2008). To determine whether cells in each group were "simple" or "complex" we measured the *F1*-to-*F0* ratio at each neuron's preferred orientation (*F1/F0*$_{Pref}$; Fig. 7*C*). Neurons that have a *F1/F0* > 1 are typically considered "simple" cells and, subthreshold OSI measurements using *F1* values are most appropriate (Carandini and Ferster 2000; Niell and Stryker 2008). Almost all cells recorded had *F1/F0*$_{Pref}$ values >1, and we calculated the subthreshold OSI using either Area (Fig. 7*D*) or *F1* values (Fig. 7*E*) and compared between groups. Using *F1* values gave more highly tuned subthreshold OSI for all groups compared with subthreshold OSI using Area, but the groups were not statistically different with either measurement (Fig. 7, *D* and *E*). Finally, we calculated the DSI for the subthreshold responses (Area), and this measurement was not different between groups (Fig. 7*F*).

Together, these data indicate that *Ube3a* loss broadens orientation tuning of the spiking responses in L2/3 RS neurons and has more subtle effects on subthreshold responses to orientation.

DISCUSSION

This work represents the first in vivo investigation into cellular excitability, orientation tuning, and contrast sensitivity in an AS model mouse line. We found that individual L2/3 RS

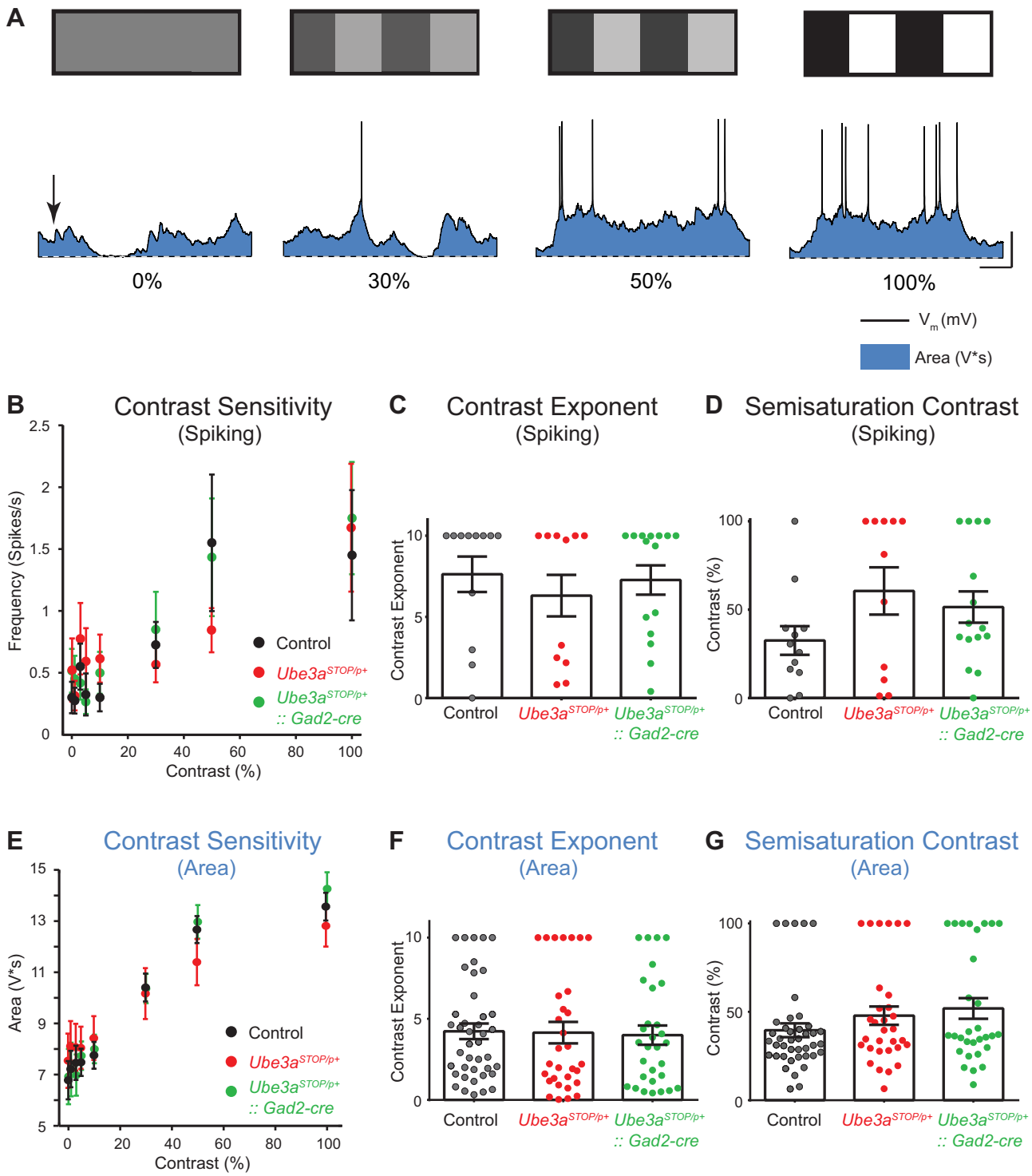

Fig. 5. Contrast sensitivity is unchanged in *Ube3a*$^{STOP/p+}$ mice. *A*: sample recording from a L2/3 RS neuron of visually evoked responses to drifting gratings of increasing contrast (scale bar 150 ms, 20 mV). Blue shaded region indicates the zone representing the "Area" measurement or subthreshold synaptic response to visual stimulation. *B*: average contrast sensitivity curves for spiking responses fit with a hyperbolic ratio equation for control (n = 12), *Ube3a*$^{STOP/p+}$ (n = 11), and *Ube3a*$^{STOP/p+}$*::Gad2-Cre* (n = 15) mice. *C*: average contrast exponent for spiking responses fit with a hyperbolic ratio equation in control (n = 12), *Ube3a*$^{STOP/p+}$ (n = 11), and *Ube3a*$^{STOP/p+}$*:: Gad2-Cre* (n = 15) mice (Kruskal-Wallis test, P = 0.311). *D*: average semisaturation contrast (C_{50}) for spiking responses fit with a hyperbolic ratio equation in control (n = 12), *Ube3a*$^{STOP/p+}$ (n = 11), and *Ube3a*$^{STOP/p+}$*::Gad2-Cre* (n = 15) mice (Kruskal-Wallis test, P = 0.300). *E*: average contrast sensitivity curves for subthreshold responses fit with a hyperbolic ratio equation for control (n = 41), *Ube3a*$^{STOP/p+}$ (n = 31), and *Ube3a*$^{STOP/p+}$*::Gad2-Cre* (n = 30) mice. *F*: average contrast exponent for subthreshold responses fit with a hyperbolic ratio equation in control (n = 41), *Ube3a*$^{STOP/p+}$ (n = 31), and *Ube3a*$^{STOP/p+}$*::Gad2-Cre* (n = 30) mice (Kruskal-Wallis test, P = 0.800). *G*: average semisaturation contrast (C_{50}) for subthreshold responses fit with a hyperbolic ratio equation in control (n = 41), *Ube3a*$^{STOP/p+}$ (n = 31), and *Ube3a*$^{STOP/p+}$*::Gad2-Cre* (n = 30) mice (Kruskal-Wallis test, P = 0.238).

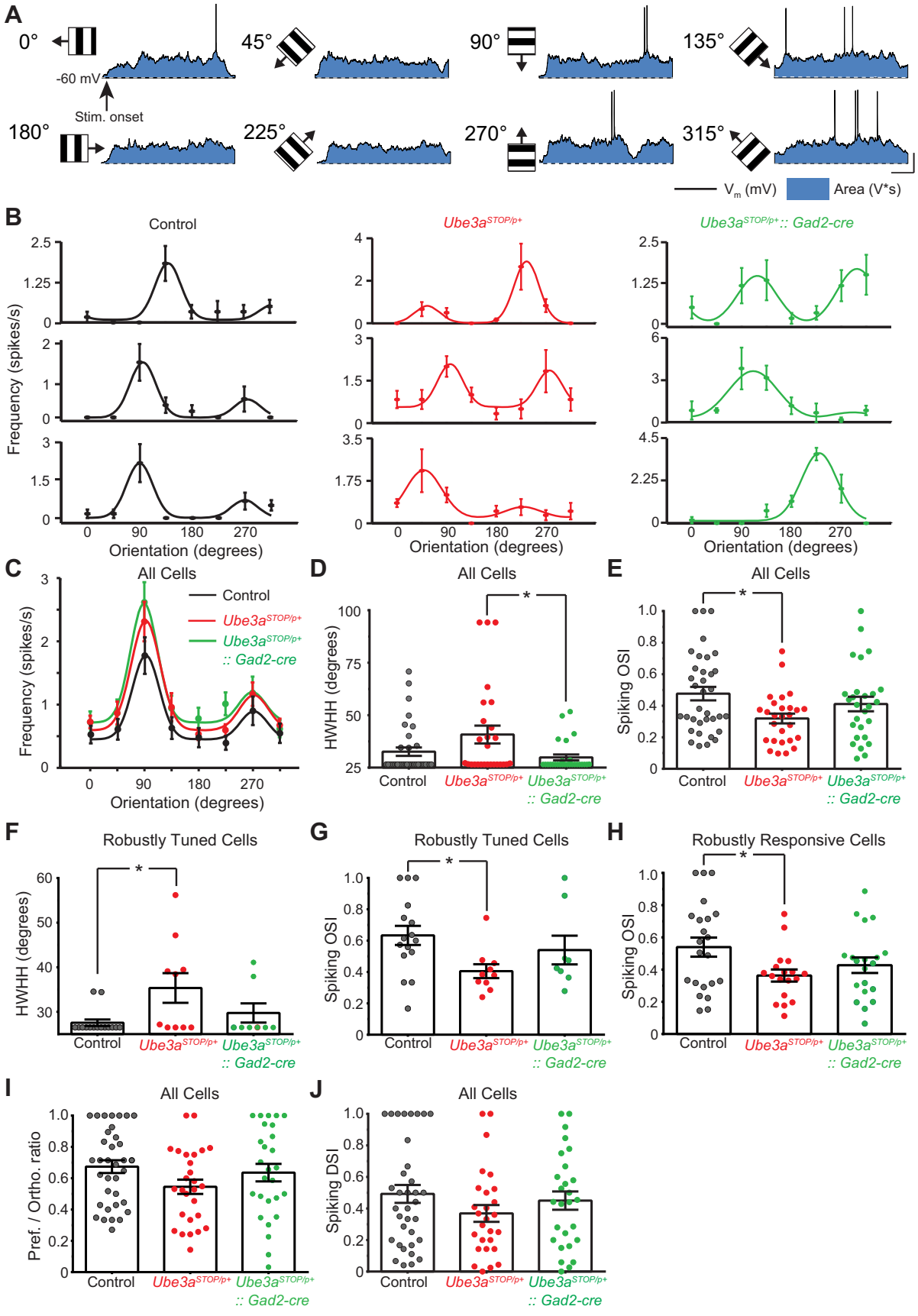

neurons had increased excitability in *Ube3a*$^{STOP/p+}$ mice but increased excitability caused by *Ube3a* loss did not translate into increased activity of the local network as measured by UP/DOWN states or spontaneous spiking. Surprisingly, increased excitability in individual neurons was rescued by reinstatement of *Ube3a* in GABAergic neurons, suggesting that a homeostatic mechanism may underlie this phenotype. A rearrangement in excitation-to-inhibition ratio that causes a net decrease in spiking may result in increased intrinsic excitability to normalize spiking rates (Nataraj et al. 2010). A decrease in excitatory synapses occurs early in development in AS model mice and may provide a period of decreased cortical spiking that is then compensated for by the observed increase in pyramidal neuron intrinsic excitability that fails to normalize in adulthood (Fig. 1) (Yashiro et al. 2005). Accordingly, reinstatement of *Ube3a* in GABAergic neurons may normalize network spiking levels early in postnatal development and prevent subsequent homeostatic rearrangements from occurring. Alternatively, increased intrinsic excitability in pyramidal neurons in the *Ube3a*$^{STOP/p+}$ mice may result directly from decreased tonic (rather than phasic/evoked) inhibition leading to increased membrane resistance. We previously showed that *Ube3a*-deficient L2/3 pyramidal neurons have decreased tonic inhibition (Judson et al. 2016). If decreased tonic inhibition underlies increased intrinsic excitability, then we would predict normal levels of tonic inhibition to be restored in the *Ube3a*^{STOP}*::Gad2-Cre* mice.

We also measured membrane potential oscillations in active (during visual stimulation) and inactive (in the absence of visual stimulation) states by comparing power spectra between genotypes (Figs. 3 and 4). Visual stimulation greatly increased spectral power in the gamma band, but we did not observe differences in spectral power between genotypes either during baseline conditions or with visual stimulation. We were surprised by this finding because both AS model mice and individuals with AS have EEG abnormalities, particularly in the delta band (Judson et al. 2016; Miura et al. 2002; Thibert et al. 2013). As anesthesia significantly increases activity in the delta band, we suspect that differences in delta band activity were masked in our recordings in anesthetized mice (Pagliardini et al. 2013). Therefore, it is possible that recordings in awake animals may expose additional differences in network excitability, especially since anesthetics have been shown to alter inhibitory neuron function in the visual system (Haider et al. 2013). Alternatively, it is possible that the enhanced delta activity previously observed with EEG and LFP recordings might manifest from activity in cell types other than L2/3 RS neurons.

We examined two visual cortical response properties, orientation selectivity and contrast sensitivity, in the AS model mice at both the spiking and subthreshold levels (Figs. 5–7). We found that both subthreshold and spiking responses to drifting grating stimuli presented at different contrasts were similar between genotypes. However, spiking responses to drifting gratings of different orientations were more broadly tuned in *Ube3a*$^{STOP/p+}$ mice than in control mice. Furthermore, reinstating *Ube3a* in GABAergic neurons in *Ube3a*$^{STOP/p+}$*::Gad2*-Cre mice partially ameliorated this phenotype, as tuning indexes from *Ube3a*$^{STOP/p+}$*::Gad2*-Cre mice were not statistically different from control mice. Subthreshold orientation tuning curves in *Ube3a*$^{STOP/p+}$ mice also showed a trend for having more broadly tuned responses; however, these changes did not reach statistical significance in our sample size.

Previous studies have suggested that sensitivity to contrast arises early in the visual system at the level of retinal ganglion cells (Shapley 1990; Shapley and Victor 1978). Our negative results with respect to contrast sensitivity suggest that the function of visual circuits remains largely intact in AS model mice at the retinal and thalamic stages. This is consistent with our work and work from others demonstrating normal visual acuity and retinotopy in AS model mice (Sato and Stryker 2010; Yashiro et al. 2009). Therefore, the orientation tuning defects we observed in this study appear to be somewhat specific in regard to visual system dysfunction in AS. Interestingly, defects in orientation tuning were only observed in spiking responses and not in subthreshold tuning curves. We examined subthreshold tuning by measuring the area between the membrane potential response and the average "DOWN" state membrane potential as well as using the *F1*-to-*F0* ratio. While OSI was increased with *F1/F0* measurements compared with area measurements, neither metric revealed a defect in subthreshold orientation tuning that was statistically distinguishable. It is currently difficult to discern the mechanism underlying broader orientation tuning in RS neurons in *Ube3a*^{STOP} mice. L2/3 pyramidal neurons in *Ube3a*^{STOP} mice do have decreased evoked inhibitory input (Judson et al. 2016), and decreasing inhibition onto pyramidal neurons has been shown to decrease orientation selectivity (Atallah et al. 2012;

Fig. 6. Broader orientation tuning in L2/3 regular spiking neurons of *Ube3a*$^{STOP/p+}$ mice. *A*: sample recording from a L2/3 RS neuron to drifting gratings of different orientations. Blue shaded region indicates the zone representing the "Area" measurement or subthreshold synaptic response to visual stimulation (note that this neuron did not show significant subthreshold *F1* modulation) (scale bar 200 ms, 20 mV). *B*: sample tuning curves and spiking responses to visual stimuli of different orientations (3 sample neurons per group) for control (*left*, black), *Ube3a*$^{STOP/p+}$ (*center*, red), and *Ube3a*$^{STOP/p+}$*::Gad2-Cre* (*right*, green) mice. Spiking responses are represented as mean ± SE of at least 6 presentations of each orientation. Tuning curve for sample recording (*A*) is top rightmost curve of the samples from the *Ube3a*$^{STOP/p+}$*::Gad2-Cre* group. *C*: average tuning curves from control ($n = 35$), *Ube3a*$^{STOP/p+}$ ($n = 27$), and *Ube3a*$^{STOP/p+}$*::Gad2-Cre* ($n = 27$) mice. *D*: half-width at half-height (HWHH) measurements made from Gaussian fits of spiking orientation tuning curves from control ($n = 35$), *Ube3a*$^{STOP/p+}$ ($n = 27$), and *Ube3a*$^{STOP/p+}$*::Gad2-Cre* ($n = 27$) mice (Kruskal-Wallis test, $P = 0.041$). *E*: orientation selectivity index (OSI) measured from spiking orientation tuning curves from all recorded cells in control ($n = 35$), *Ube3a*$^{STOP/p+}$ ($n = 27$), and *Ube3a*$^{STOP/p+}$*:: Gad2-Cre* ($n = 27$) mice (ANOVA, $P = 0.026$). *F*: HWHH measurements made from Gaussian fits of spiking orientation tuning curves for robustly tuned cells in control ($n = 15$), *Ube3a*$^{STOP/p+}$ ($n = 10$), and *Ube3a*$^{STOP/p+}$*::Gad2-Cre* ($n = 8$) mice (Kruskal-Wallis test, $P = 0.044$). *G*: OSI measured from spiking responses from cells that were well fit by sum-of-two-Gaussian tuning curves [i.e., normalized residuals of the fit were <0.0125; control ($n = 16$), *Ube3a*$^{STOP/p+}$ ($n = 10$), and *Ube3a*$^{STOP/p+}$*::Gad2-Cre* ($n = 8$), Kruskal-Wallis test, $P = 0.031$]. *H*: OSI measured from spiking orientation tuning curves from cells that robustly responded to at least 1 orientation compared with all others [i.e., ANOVA post-hoc test must be $P < 0.05$; control ($n = 22$), *Ube3a*$^{STOP/p+}$ ($n = 18$), and *Ube3a*$^{STOP/p+}$*:: Gad2-Cre* ($n = 20$), ANOVA, $P = 0.045$]. *I*: preferred-to-orthogonal ratio from spiking orientation tuning curves from all recorded cells in control ($n = 35$), *Ube3a*$^{STOP/p+}$ ($n = 27$), and *Ube3a*$^{STOP/p+}$*:: Gad2-Cre* ($n = 27$) mice (Kruskal-Wallis test, $P = 0.151$). *J*: direction selectivity index (DSI) measured from spiking orientation tuning curves from all recorded cells in control ($n = 35$), *Ube3a*$^{STOP/p+}$ ($n = 27$), and *Ube3a*$^{STOP/p+}$*::Gad2-Cre* ($n = 27$) mice (ANOVA, $P = 0.294$). *$P < 0.05$ with post hoc test for significance.

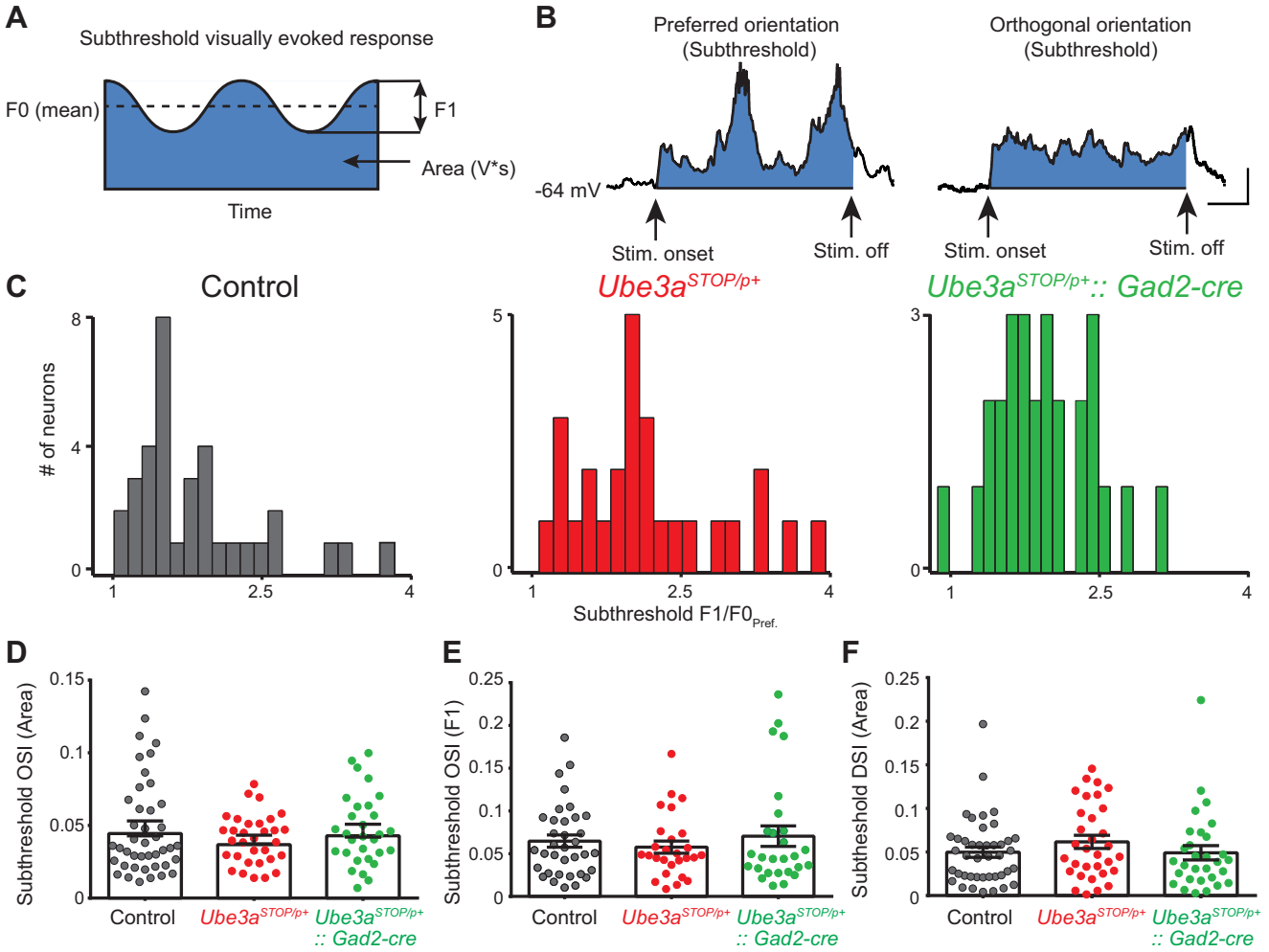

Fig. 7. Subthreshold orientation tuning is unchanged in *Ube3a*$^{STOP/p+}$ mice. *A*: illustration of the measurements made for the subthreshold analysis of visual responses. *F0* is the mean subthreshold membrane potential, *F1* is the difference between the peak and trough of the subthreshold membrane potential, and blue shaded region corresponds to the Area ($V \times s$) measurement. All measurements are made during presentation of the visual stimulus. *B*: sample recording from a L2/3 RS neuron to drifting gratings in its preferred and orthogonal orientations. Blue shaded region indicates the zone representing the "Area" measurement or subthreshold synaptic response to visual stimulation. The recordings are averages of 6 presentations of the same orientation and low-pass filtered at 100 Hz. (note that this neuron had significant subthreshold *F1* modulation to the preferred orientation) (scale bar 200 ms, 5 mV). *C*: histograms of subthreshold *F1/F0* measurements at the neuron's preferred orientation ($F1/F0_{Pref}$). *D*: orientation selectivity index measured from subthreshold (Area) orientation tuning curves from control ($n = 42$), *Ube3a*$^{STOP/p+}$ ($n = 32$), and *Ube3a*$^{STOP/p+}$*::Gad2-Cre* ($n = 30$) mice (Kruskal-Wallis test, $P = 0.774$). *E*: orientation selectivity index measured from subthreshold *F1* from control ($n = 35$), *Ube3a*$^{STOP/p+}$ ($n = 27$), and *Ube3a*$^{STOP/p+}$*::Gad2-Cre* ($n = 27$) mice (Kruskal-Wallis test, $P = 0.85$). *F*: direction selectivity index measured from subthreshold (Area) orientation tuning curves from control ($n = 42$), *Ube3a*$^{STOP/p+}$ ($n = 32$), and *Ube3a*$^{STOP/p+}$*::Gad2-Cre* ($n = 30$) mice (ANOVA, $P = 0.393$).

Wilson et al. 2012). Interestingly, reinstating *Ube3a* in GABAergic neurons in *Ube3a*^{STOP}*::Gad2-Cre* mice also results in an intermediate effect on evoked inhibition, indicating that a lack of a robust "rescue" of orientation selectivity in *Ube3a*^{STOP}*::Gad2-Cre* mice may reflect the intermediate effect in evoked inhibition (Judson et al. 2016). Of course, there are many other synaptic and circuit contributions to orientation tuning that could be defective in *Ube3a*^{STOP} mice, such as the tuning of thalamic input, changes in excitability, or receptive field structure (Priebe and Ferster 2012).

Overall, this work demonstrates that maternal *Ube3a* loss disrupts cortex-dependent computations. Specifically, excitability is higher in L2/3 RS neurons in the visual cortex of AS model mice in vivo, and orientation selectivity is weaker, compared with control littermates. Surprisingly, our data indicate that reinstatement of *Ube3a* in GABAergic neurons alone results in normal excitability and orientation tuning. This is congruent with recent findings demonstrating that reinstatement of *Ube3a* in GABAergic neurons can also normalize seizure susceptibility and elevated delta band EEG activity in AS model mice (Judson et al. 2016). Together these studies point to a critical role for *Ube3a* in GABAergic neurons in the pathogenesis of AS and suggest that reinstatement of *Ube3a* in GABAergic neurons may have a wide range of therapeutic benefits.

ACKNOWLEDGMENTS

We thank M. Carandini for providing the MATLAB code to fit orientation tuning and contrast response curves; K. Sellers and F. Frohlich for providing the MATLAB code for spectral analysis; J. Han for genotyping and imaging support; M. Judson, R. Larsen, and J. Berrios for experimental advice; and P. Manis for his expertise and advice on data analysis.

Present address of M. L. Wallace: Howard Hughes Medical Institute, Dept. of Neurobiology, Harvard Medical School, Boston, MA 02115.

GRANTS

This work was supported by National Institute of Neurological Disorders and Stroke (NINDS) NRSA Fellowship 1F31 NS-077847 (M. L. Wallace); the Angelman Syndrome Foundation, Simons Foundation Grant SFARI no. 274426, and NINDS Grant R01 NS-085093 (B. D. Philpot); the Angelman Syndrome Foundation and NWO-ZoN-Mw grant (Y. Elgersma); an EMC fellowship (G. M. van Woerden); and grants from the Whitehall Foundation and the Klingenstein Foundation, Simons Foundation Grant SCGB 325407SS, National Science Foundation Grant 1450824, and NINDS Grant 1R01 NS-091335 (S. L. Smith).

DISCLOSURES

No conflicts of interest, financial or otherwise, are declared by the authors.

AUTHOR CONTRIBUTIONS

M.L.W., S.L.S., and B.D.P. conceived and designed research; M.L.W. performed experiments; M.L.W., S.L.S., and B.D.P. analyzed data; M.L.W., S.L.S., and B.D.P. interpreted results of experiments; M.L.W., S.L.S., and B.D.P. prepared figures; M.L.W., S.L.S., and B.D.P. drafted manuscript; M.L.W., G.M.v.W., Y.E., S.L.S., and B.D.P. edited and revised manuscript; M.L.W., G.M.v.W., Y.E., S.L.S., and B.D.P. approved final version of manuscript.

REFERENCES

Albrecht DG, Hamilton DB. Striate cortex of monkey and cat: contrast response function. *J Neurophysiol* 48: 217–237, 1982.

Atallah BV, Bruns W, Carandini M, Scanziani M. Parvalbumin-expressing interneurons linearly transform cortical responses to visual stimuli. *Neuron* 73: 159–170, 2012. doi:10.1016/j.neuron.2011.12.013.

Beltramo R, D'Urso G, Dal Maschio M, Farisello P, Bovetti S, Clovis Y, Lassi G, Tucci V, De Pietri Tonelli D, Fellin T. Layer-specific excitatory circuits differentially control recurrent network dynamics in the neocortex. *Nat Neurosci* 16: 227–234, 2013. doi:10.1038/nn.3306.

Brainard DH. The Psychophysics Toolbox. *Spat Vis* 10: 433–436, 1997. doi:10.1163/156856897X00357.

Carandini M, Ferster D. Membrane potential and firing rate in cat primary visual cortex. *J Neurosci* 20: 470–484, 2000.

Cardin JA, Carlén M, Meletis K, Knoblich U, Zhang F, Deisseroth K, Tsai LH, Moore CI. Driving fast-spiking cells induces gamma rhythm and controls sensory responses. *Nature* 459: 663–667, 2009. doi:10.1038/nature08002.

Colas D, Wagstaff J, Fort P, Salvert D, Sarda N. Sleep disturbances in Ube3a maternal-deficient mice modeling Angelman syndrome. *Neurobiol Dis* 20: 471–478, 2005. doi:10.1016/j.nbd.2005.04.003.

Cottam JC, Smith SL, Häusser M. Target-specific effects of somatostatin-expressing interneurons on neocortical visual processing. *J Neurosci* 33: 19567–19578, 2013. doi:10.1523/JNEUROSCI.2624-13.2013.

de Kock CP, Bruno RM, Spors H, Sakmann B. Layer- and cell-type-specific suprathreshold stimulus representation in rat primary somatosensory cortex. *J Physiol* 581: 139–154, 2007. doi:10.1113/jphysiol.2006.124321.

Eckhorn R, Bauer R, Jordan W, Brosch M, Kruse W, Munk M, Reitboeck HJ. Coherent oscillations: a mechanism of feature linking in the visual cortex? Multiple electrode and correlation analyses in the cat. *Biol Cybern* 60: 121–130, 1988. doi:10.1007/BF00202899.

Gibson JR, Bartley AF, Hays SA, Huber KM. Imbalance of neocortical excitation and inhibition and altered UP states reflect network hyperexcitability in the mouse model of fragile X syndrome. *J Neurophysiol* 100: 2615–2626, 2008. doi:10.1152/jn.90752.2008.

Gonçalves JT, Anstey JE, Golshani P, Portera-Cailliau C. Circuit level defects in the developing neocortex of Fragile X mice. *Nat Neurosci* 16: 903–909, 2013. doi:10.1038/nn.3415.

Goupillaud P, Grossmann A, Morlet J. Cycle-octave and related transforms in seismic signal analysis. *Geoexploration* 23: 85–102, 1984. doi:10.1016/0016-7142(84)90025-5.

Haider B, Häusser M, Carandini M. Inhibition dominates sensory responses in the awake cortex. *Nature* 493: 97–100, 2013. doi:10.1038/nature11665.

Haider B, McCormick DA. Rapid neocortical dynamics: cellular and network mechanisms. *Neuron* 62: 171–189, 2009. doi:10.1016/j.neuron.2009.04.008.

Hays SA, Huber KM, Gibson JR. Altered neocortical rhythmic activity states in Fmr1 KO mice are due to enhanced mGluR5 signaling and involve changes in excitatory circuitry. *J Neurosci* 31: 14223–14234, 2011. doi:10.1523/JNEUROSCI.3157-11.2011.

Hensch TK, Fagiolini M, Mataga N, Stryker MP, Baekkeskov S, Kash SF. Local GABA circuit control of experience-dependent plasticity in developing visual cortex. *Science* 282: 1504–1508, 1998. doi:10.1126/science.282.5393.1504.

Hubel DH, Wiesel TN. Integrative action in the cat's lateral geniculate body. *J Physiol* 155: 385–398, 1961. doi:10.1113/jphysiol.1961.sp006635.

Hubel DH, Wiesel TN. Receptive fields, binocular interaction and functional architecture in the cat's visual cortex. *J Physiol* 160: 106–154, 1962. doi:10.1113/jphysiol.1962.sp006837.

Isaacson JS, Scanziani M. How inhibition shapes cortical activity. *Neuron* 72: 231–243, 2011. doi:10.1016/j.neuron.2011.09.027.

Jiang YH, Armstrong D, Albrecht U, Atkins CM, Noebels JL, Eichele G, Sweatt JD, Beaudet AL. Mutation of the Angelman ubiquitin ligase in mice causes increased cytoplasmic p53 and deficits of contextual learning and long-term potentiation. *Neuron* 21: 799–811, 1998. doi:10.1016/S0896-6273(00)80596-6.

Judson MC, Wallace ML, Sidorov MS, Burette AC, Gu B, van Woerden GM, King IF, Han JE, Zylka MJ, Elgersma Y, Weinberg RJ, Philpot BD. GABAergic neuron-specific loss of Ube3a causes Angelman syndrome-like EEG abnormalities and enhances seizure susceptibility. *Neuron* 90: 56–69, 2016. doi:10.1016/j.neuron.2016.02.040.

Kishino T, Lalande M, Wagstaff J. UBE3A/E6-AP mutations cause Angelman syndrome. *Nat Genet* 15: 70–73, 1997. doi:10.1038/ng0197-70.

Lee SH, Kwan AC, Zhang S, Phoumthipphavong V, Flannery JG, Masmanidis SC, Taniguchi H, Huang ZJ, Zhang F, Boyden ES, Deisseroth K, Dan Y. Activation of specific interneurons improves V1 feature selectivity and visual perception. *Nature* 488: 379–383, 2012. doi:10.1038/nature11312.

Lien AD, Scanziani M. Tuned thalamic excitation is amplified by visual cortical circuits. *Nat Neurosci* 16: 1315–1323, 2013. doi:10.1038/nn.3488.

Margrie TW, Brecht M, Sakmann B. In vivo, low-resistance, whole-cell recordings from neurons in the anaesthetized and awake mammalian brain. *Pflugers Arch* 444: 491–498, 2002. doi:10.1007/s00424-002-0831-z.

Miura K, Kishino T, Li E, Webber H, Dikkes P, Holmes GL, Wagstaff J. Neurobehavioral and electroencephalographic abnormalities in Ube3a maternal-deficient mice. *Neurobiol Dis* 9: 149–159, 2002. doi:10.1006/nbdi.2001.0463.

Nataraj K, Le Roux N, Nahmani M, Lefort S, Turrigiano G. Visual deprivation suppresses L5 pyramidal neuron excitability by preventing the induction of intrinsic plasticity. *Neuron* 68: 750–762, 2010. doi:10.1016/j.neuron.2010.09.033.

Niell CM, Stryker MP. Highly selective receptive fields in mouse visual cortex. *J Neurosci* 28: 7520–7536, 2008. doi:10.1523/JNEUROSCI.0623-08.2008.

Orekhova EV, Stroganova TA, Nygren G, Tsetlin MM, Posikera IN, Gillberg C, Elam M. Excess of high frequency electroencephalogram oscillations in boys with autism. *Biol Psychiatry* 62: 1022–1029, 2007. doi:10.1016/j.biopsych.2006.12.029.

Pagliardini S, Funk GD, Dickson CT. Breathing and brain state: urethane anesthesia as a model for natural sleep. *Respir Physiol Neurobiol* 188: 324–332, 2013. doi:10.1016/j.resp.2013.05.035.

Paluszkiewicz SM, Olmos-Serrano JL, Corbin JG, Huntsman MM. Impaired inhibitory control of cortical synchronization in fragile X syndrome. *J Neurophysiol* 106: 2264–2272, 2011. doi:10.1152/jn.00421.2011.

Poulet JF, Petersen CC. Internal brain state regulates membrane potential synchrony in barrel cortex of behaving mice. *Nature* 454: 881–885, 2008. doi:10.1038/nature07150.

Priebe NJ, Ferster D. Mechanisms of neuronal computation in mammalian visual cortex. *Neuron* 75: 194–208, 2012. doi:10.1016/j.neuron.2012.06.011.

Ringach DL, Hawken MJ, Shapley R. Dynamics of orientation tuning in macaque primary visual cortex. *Nature* 387: 281–284, 1997. doi:10.1038/387281a0.

Sanchez-Vives MV, McCormick DA. Cellular and network mechanisms of rhythmic recurrent activity in neocortex. *Nat Neurosci* 3: 1027–1034, 2000. doi:10.1038/79848.

Sato M, Stryker MP. Genomic imprinting of experience-dependent cortical plasticity by the ubiquitin ligase gene Ube3a. *Proc Natl Acad Sci USA* 107: 5611–5616, 2010. doi:10.1073/pnas.1001281107.

Sellers KK, Bennett DV, Hutt A, Fröhlich F. Anesthesia differentially modulates spontaneous network dynamics by cortical area and layer. *J Neurophysiol* 110: 2739–2751, 2013. doi:10.1152/jn.00404.2013.

Shapley R. Visual sensitivity and parallel retinocortical channels. *Annu Rev Psychol* 41: 635–658, 1990. doi:10.1146/annurev.ps.41.020190.003223.

Shapley RM, Victor JD. The effect of contrast on the transfer properties of cat retinal ganglion cells. *J Physiol* 285: 275–298, 1978. doi:10.1113/jphysiol.1978.sp012571.

Shu Y, Hasenstaub A, McCormick DA. Turning on and off recurrent balanced cortical activity. *Nature* 423: 288–293, 2003. doi:10.1038/nature01616.

Silva-Santos S, van Woerden GM, Bruinsma CF, Mientjes E, Jolfaei MA, Distel B, Kushner SA, Elgersma Y. Ube3a reinstatement identifies distinct developmental windows in a murine Angelman syndrome model. *J Clin Invest* 125: 2069–2076, 2015. doi:10.1172/JCI80554.

Smith SL, Smith IT, Branco T, Häusser M. Dendritic spikes enhance stimulus selectivity in cortical neurons in vivo. *Nature* 503: 115–120, 2013. doi:10.1038/nature12600.

Sohal VS, Zhang F, Yizhar O, Deisseroth K. Parvalbumin neurons and gamma rhythms enhance cortical circuit performance. *Nature* 459: 698–702, 2009. doi:10.1038/nature07991.

Steriade M, Nuñez A, Amzica F. A novel slow (<1 Hz) oscillation of neocortical neurons in vivo: depolarizing and hyperpolarizing components. *J Neurosci* 13: 3252–3265, 1993.

Taniguchi H, He M, Wu P, Kim S, Paik R, Sugino K, Kvitsiani D, Fu Y, Lu J, Lin Y, Miyoshi G, Shima Y, Fishell G, Nelson SB, Huang ZJ. A resource of Cre driver lines for genetic targeting of GABAergic neurons in cerebral cortex. *Neuron* 71: 995–1013, 2011. doi:10.1016/j.neuron.2011.07.026.

Thibert RL, Larson AM, Hsieh DT, Raby AR, Thiele EA. Neurologic manifestations of Angelman syndrome. *Pediatr Neurol* 48: 271–279, 2013. doi:10.1016/j.pediatrneurol.2012.09.015.

Wallace ML, Burette AC, Weinberg RJ, Philpot BD. Maternal loss of Ube3a produces an excitatory/inhibitory imbalance through neuron type-specific synaptic defects. *Neuron* 74: 793–800, 2012. doi:10.1016/j.neuron.2012.03.036.

Williams CA, Beaudet AL, Clayton-Smith J, Knoll JH, Kyllerman M, Laan LA, Magenis RE, Moncla A, Schinzel AA, Summers JA, Wagstaff J. Angelman syndrome 2005: updated consensus for diagnostic criteria. *Am J Med Genet A* 140: 413–418, 2006. doi:10.1002/ajmg.a.31074.

Wilson NR, Runyan CA, Wang FL, Sur M. Division and subtraction by distinct cortical inhibitory networks in vivo. *Nature* 488: 343–348, 2012. doi:10.1038/nature11347.

Wolfe J, Houweling AR, Brecht M. Sparse and powerful cortical spikes. *Curr Opin Neurobiol* 20: 306–312, 2010. doi:10.1016/j.conb.2010.03.006.

Yashiro K, Corlew R, Philpot BD. Visual deprivation modifies both presynaptic glutamate release and the composition of perisynaptic/extrasynaptic NMDA receptors in adult visual cortex. *J Neurosci* 25: 11684–11692, 2005. doi:10.1523/JNEUROSCI.4362-05.2005.

Yashiro K, Riday TT, Condon KH, Roberts AC, Bernardo DR, Prakash R, Weinberg RJ, Ehlers MD, Philpot BD. Ube3a is required for experience-dependent maturation of the neocortex. *Nat Neurosci* 12: 777–783, 2009. doi:10.1038/nn.2327.